

See discussions, stats, and author profiles for this publication at: <https://www.researchgate.net/publication/258850521>

# Influence of Acoustic Cavitation on the Controlled Ultrasonic Dispersion of Carbon Nanotubes

ARTICLE *in* THE JOURNAL OF PHYSICAL CHEMISTRY B · NOVEMBER 2013

Impact Factor: 3.3 · DOI: 10.1021/jp410041y · Source: PubMed

---

CITATIONS

12

READS

70

## 8 AUTHORS, INCLUDING:



Achilleas Sesis

2 PUBLICATIONS 12 CITATIONS

[SEE PROFILE](#)



Gianluca Memoli

National Physical Laboratory

36 PUBLICATIONS 186 CITATIONS

[SEE PROFILE](#)



Alan B Dalton

University of Surrey

119 PUBLICATIONS 5,253 CITATIONS

[SEE PROFILE](#)



J David Carey

University of Surrey

114 PUBLICATIONS 1,838 CITATIONS

[SEE PROFILE](#)

# Influence of Acoustic Cavitation on the Controlled Ultrasonic Dispersion of Carbon Nanotubes

Achilleas Sesis,<sup>†</sup> Mark Hodnett,<sup>†</sup> Gianluca Memoli,<sup>†</sup> Andrew J. Wain,<sup>†</sup> Izabela Jurewicz,<sup>‡</sup> Alan B. Dalton,<sup>‡</sup> J. David Carey,<sup>§</sup> and Gareth Hinds\*,<sup>†</sup>

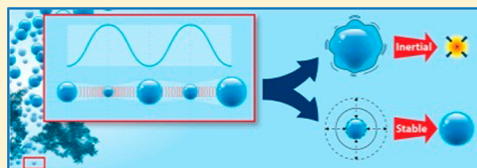
<sup>†</sup>National Physical Laboratory, Teddington, Middlesex TW11 0LW, United Kingdom

<sup>‡</sup>Department of Physics, University of Surrey, Guildford, Surrey GU2 7XH, United Kingdom

<sup>§</sup>Advanced Technology Institute, University of Surrey, Guildford, Surrey GU2 7XH, United Kingdom

## S Supporting Information

**ABSTRACT:** Ultrasonication is the most widely used technique for the dispersion of a range of nanomaterials, but the intrinsic mechanism which leads to stable solutions is poorly understood with procedures quoted in the literature typically specifying only extrinsic parameters such as nominal electrical input power and exposure time. Here we present new insights into the dispersion mechanism of a representative nanomaterial, single-walled carbon nanotubes (SW-CNTs), using a novel up-scalable sonoreactor and an *in situ* technique for the measurement of acoustic cavitation activity during ultrasonication. We distinguish between stable cavitation, which leads to chemical modification of the surface of the CNTs, and inertial cavitation, which favors CNT exfoliation and length reduction. Efficient dispersion of CNTs in aqueous solution is found to be dominated by mechanical forces generated via inertial cavitation, which in turn depends critically on surfactant concentration. This study highlights that careful measurement and control of cavitation rather than blind application of input power is essential in the large volume production of nanomaterial dispersions with tailored properties.



## A. INTRODUCTION

A key area of nanotechnology development is the processing of functional nanomaterials.<sup>1,2</sup> Single-walled carbon nanotubes (SW-CNTs) have come to represent the prototype high aspect ratio nanomaterial and have been extensively studied due to their remarkable mechanical and electrical properties<sup>3</sup> for a wide range of potential applications<sup>4</sup> in biotechnology, composites, and electronics. To take advantage of their intrinsic nanoscale properties in macroscale structures or devices, individually dispersed CNTs or small bundles are usually required. A significant material processing hurdle for CNTs, and other nanomaterials such as graphene, is the requirement to eliminate their strong tendency to agglomerate due to van der Waals interactions.<sup>5</sup> The primary chemical approach to stabilizing CNT dispersions is through the use of an appropriate solvent,<sup>6</sup> with aqueous dispersions typically requiring an effective surfactant. A wide range of types of surfactant and concentrations has been investigated in the literature with various dispersion outcomes depending on the specific processes.<sup>7</sup>

Ultrasonication has emerged as the prevailing technique for the dispersion of a range of nanomaterials. During ultrasonic processing in liquids the propagation of high amplitude ultrasonic pressure waves, typically generated using frequencies between 20 kHz and 1 MHz, leads to molecular dissociation, void creation, and the rapid formation of cavities (bubbles). Continued interaction between bubbles and the acoustic field can result in their growth and, ultimately, violent collapse. The

implosion of bubbles can create local temperatures of several thousand kelvin and pressures of several hundred atmospheres.<sup>8</sup> During the growth and collapse phases sonochemical effects will occur, while extreme shear forces as well as optical and acoustic emissions are also generated.<sup>9,10</sup> Cavitation is a complex multiparametric phenomenon that depends on the physicochemical properties of the liquid and the operational parameters of the ultrasonic device.<sup>11</sup> Studies of single-bubble interactions with CNTs have been limited to computational modeling,<sup>12</sup> while more realistic multibubble systems have not been addressed. Until now, the effectiveness of ultrasonic dispersion has only been characterized by postprocessing analysis of the CNTs<sup>13</sup> as a definitive metric for cavitation was not available.

Despite its critical role in the dispersion process, the fundamental mechanism of ultrasonic dispersion in complex environments is poorly understood, and the role of acoustic cavitation is often neglected by the materials science community. As a consequence, many of the dispersion strategies in the literature are empirical in nature and typically specify only the solute concentrations, the nominal electrical input power of the device, and the exposure time. Moreover, this type of treatment may lead to unintentional and undesirable chemical and physical modification of the

Received: October 9, 2013

Revised: November 14, 2013

Published: November 19, 2013

CNTs.<sup>14</sup> The need for a more systematic approach to the dispersion of nanomaterials and nanoparticles has been highlighted in a recent review article.<sup>15</sup>

On the other hand, the effects of acoustic cavitation can be monitored directly in near real-time using techniques such as sonoluminescence and acoustic emission or indirectly by evaluating the yield of chemical byproducts and monitoring erosion of surfaces.<sup>11</sup> With bubbles in solution behaving as secondary sound sources, it is possible to interpret the acoustic emission spectra in terms of bubble growth and implosion behavior<sup>10</sup> and therefore link a macroscopic signal to what is happening at the nanoscale. In this context, the National Physical Laboratory (NPL) has pioneered the development of a reference cavitation facility<sup>16</sup> to understand the underlying physics of cavitation.

In this work we apply a modified NPL cavitation sensor<sup>17</sup> to the *in situ* investigation of the fundamental CNT dispersion mechanisms. We demonstrate unequivocally the importance of cavitation activity measurement and the identification of the cavitation type, for understanding and controlling the dispersion of CNTs. The effects of ultrasonication on the surfactant as well as a means to controllably adjust the nanotube length are also examined. Our conclusions are not limited to carbon nanotubes and can be applied to any nanomaterial systems in which van der Waal interactions are important.

## B. EXPERIMENTAL SECTION

**Solution Preparation.** Air-saturated stock solutions of 0.72 mM (30% cmc) and 7.2 mM (300% cmc) of sodium deoxycholate (NaDOC) (Thermo Scientific) in Milli-Q water (18.2 MΩ cm, < 5 ppb T.O.C.) were prepared prior to each experiment by magnetic stirring at 1000 rpm for 1 h at 25 °C. Prior to the cavitation measurements 10 mL aliquots of the stock solution were ultrasonicated in a 15 mL polypropylene nonskirted centrifugation tube (Fisher Scientific) in the 25 kHz reference vessel.<sup>16</sup> In this case the tube was partly immersed up to the 15 mL mark along the central axis of the 25 L vessel and a 15 min, 100 W exposure was used. Hereafter this process is termed Pretreatment. A schematic of this configuration is shown in the Supporting Information (Figure S1a). When CNTs (SRM-2483, N.I.S.T., USA) were used, in order to accelerate the dispersion process within the reactor, a total mass of 5 mg was added to the 10 mL solution to undergo the pretreatment process. The pretreated solutions were then mixed with 240 mL of the respective stock solution to form a reactor liquid volume of 250 mL. When CNTs were used the starting concentration was 0.02 mg mL<sup>-1</sup>. At fixed intervals (0, 15, 30, and 60 min) 1 mL aliquots were extracted for chemical analysis ( $\text{H}_2\text{O}_2$ ), CNT quality, and dispersion characterization. In order to minimize the exposure time of the sensor to the acoustic field, during cavitation measurements the reactor lid was replaced with an identical lid, to which the cavitation sensor was attached.

**In Situ Measurement of Ultrasonic Cavitation and Temperature.** A modified NPL cavitation sensor was housed within the custom-built reactor at a fixed height of 35 mm from the inner side of the lid. The reactor was positioned in the vessel at a fixed height (the center of the reactor body was 40 mm below the water surface) along the central axis of the reference vessel. One row of ten equally spaced transducers around the top of the reference vessel was used to apply the acoustic field throughout this work. The nominal input power

was equally distributed between the ten transducers. During acoustic cavitation experiments the sensor was connected to a spectrum analyzer (HP3589A, Hewlett-Packard), and emission signals were recorded for an average of 128 sweeps over the frequency range 2 to 4 MHz. Integration was performed on each acquired spectrum to determine the broadband integrated energy using eq 1. The temperature of both the reactor solution and the vessel solution was also recorded at 10 s intervals using PEEK-sheathed mini T-type stainless steel 0.5 mm thermocouples (Omega Engineering) connected to a temperature data logger (MMS3000 T6VA, ISE). These thermographs were then analyzed using calorimetry to estimate the effective power dissipated within the reactor. The vessel water temperature remained in the range 33.0 ± 0.5 °C throughout the tests. Using an identical configuration the reactor was also set up to acquire data on the cavitation activity associated with a sonotrode (20 kHz, P100, Sonic Systems) with a tip diameter of 15 mm (Figure S1b). In these tests the reactor solution temperature was 26.7 ± 0.9 °C, and the volume of air-saturated Milli-Q water was 300 mL. The vertical distance between the probe tip and sensor surface was fixed at 50 mm, while the tip was centered with respect to the vial and sensor. All acoustic data were acquired over a 2 min period and averaged over four to eight independent measurements.

**$\text{H}_2\text{O}_2$  Chemical Assay.** Absorption spectroscopy (Cary 5000 UV-vis-NIR, Agilent Technology) was used to measure  $\text{H}_2\text{O}_2$  concentration in the treated solutions using a peroxide assay kit (PeroXQuant, Thermo Scientific). 50 μL of the sample was mixed with the 500 μL assay immediately after its extraction from the reactor and left to stand for 24 h at 20 °C, in airtight 10 mm disposable cuvettes (UV-Cuvette micro 8.5 mm, BRAND). The absorbance of the solution was then measured at 585 nm and compared against a calibration curve produced from samples with a known concentration of  $\text{H}_2\text{O}_2$ .

**Resonance Micro-Raman Spectroscopy.** For all ultrasonicated samples, 1 mL aliquots were left to stand for 24 h at 20 °C to allow large CNT bundles to sediment under stagnant conditions. 50 μL aliquots from the supernatant were then deposited on silicon wafer substrates and left to dry in air. For the untreated samples, measurements were conducted directly on the as-received CNT powder. For all samples an average of 10 scans at various points on the substrate was taken. The spectra were obtained using an excitation wavelength of 632.8 nm (1.96 eV), using a RM 2000 microRaman spectrometer (Renishaw). The spectral resolution was 1 cm<sup>-1</sup>, and a 50× magnification objective lens was used; the spot size diameter was estimated to be approximately 1 μm with a nominal power of 1.25 mW (25% power intensity on the sample). Calibration was performed using a silicon wafer (520.5 cm<sup>-1</sup> ± 0.5 cm<sup>-1</sup>). Spectra were background corrected by removing the silicon and surfactant intensity contributions within the G- and D-band regions of interest. The quality ratios were then evaluated on the normalized spectra.

**Absorption Spectroscopy.** Absorption spectroscopy (Cary 5000 UV-vis-NIR, Agilent Technology) was used to evaluate the dispersion efficiency and relative fraction of individual CNTs for each ultrasonication. After each exposure 1 mL of sample was removed from the reactor and left to stand for 24 h under stagnant sedimentation conditions at 20 °C. 400 μL of the supernatant was placed in airtight 10 mm disposable cuvettes (UV-Cuvette micro 15 mm, BRAND). The absorbance of the solution was then measured between 400

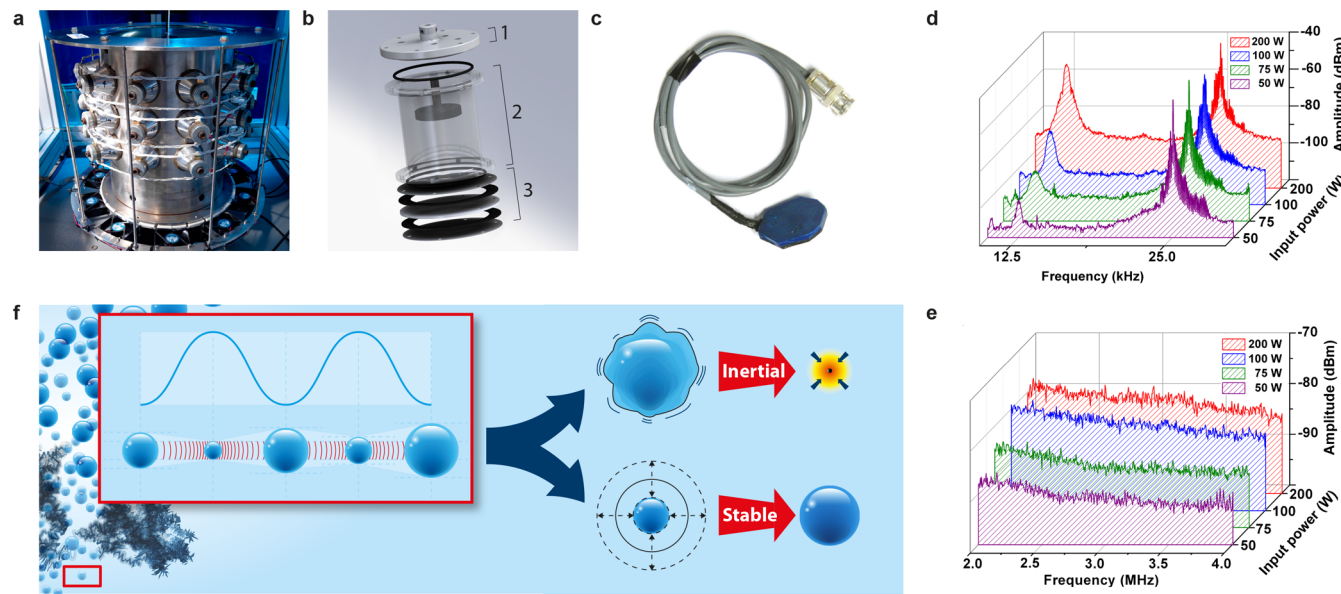


**Figure 1.** Novel experimental apparatus. **a**, NPL's 25 L, 25 kHz - frequency driven reference ultrasonic vessel. **b**, Computer-aided design of the custom-built reactor, where the lid (1) and main body (2) are made from polycarbonate and the base (3) is a ceramic-nylon sandwich layer. The maximum reactor volume is 370 mL. **c**, NPL's cavitation sensor with a thickness of 5.5 mm and a surface area of  $\sim 10 \text{ cm}^2$  housed within the reactor during experiments. **d**, Low frequency acoustic emission spectra taken with the cavitation sensor, showing the effect of input power on the  $f_0$  and  $f_0/2$  peaks as well as the broadband noise. **e**, High frequency region of the spectrum showing a clear increase of broadband noise with input power. **f**, Left: illustration of the multibubble cloud typically generated in ultrasonically treated solutions. Right: Schematic of the two types of cavitation mechanism.

and 800 nm, and the area ratio of the  $E_{22}$  resonance peak at  $\sim 570$  nm to its nonresonant background was calculated.

**Atomic Force Microscopy.** 250 mL of CNT samples was left to stand for 24 h at 20 °C to allow large CNT bundles to sediment under stagnant conditions. 40  $\mu\text{L}$  supernatant aliquots of these solutions were spin-coated at 3000 rpm for 10 s onto freshly cleaved mica substrates and left to dry in air for 15 min. For topographic studies, an NTEGRA Prima AFM (NT-MDT) was used in semicontact mode configuration. AFM probes (Nanosensors) with force constants ranging from 10 N  $\text{m}^{-1}$  to 130 N  $\text{m}^{-1}$  were used. Several AFM topography and phase images were recorded for each sample and analyzed for length and diameter distribution histograms. All images were corrected for sample tilt using NOVA (NT-MDT), and a background subtraction was employed using a first-degree polynomial plane fitting for each line scan.

**Surfactant Characterization.** Air-saturated, stock solutions of 0.12 mM (50% cmc) Triton X-100 (TX) (BioXtra, Sigma-Aldrich) and 0.048 mM (2% cmc) sodium deoxycholate (NaDOC) (Thermo Scientific) in Milli-Q water (18.2 MΩ cm, < 5 ppb T.O.C.) were prepared prior to each experiment by magnetic stirring at 1000 rpm for 1 h at 25 °C. Aliquots of 250 mL of each solution were ultrasonicated in the NPL reference vessel in the reactor using an applied nominal power of either 100 or 200 W. The vessel water temperature remained in the range  $33.0 \pm 0.5$  °C throughout the tests, and the temperature within the reactor was monitored continuously. During the ultrasonication process 1 mL aliquots were extracted from the reactor at fixed time intervals. For the TX chemical analysis a reverse phase high performance liquid chromatograph (RP-HPLC) (JASCO) with a photodiode array (PDA) UV detector set at 224 nm was used. The system was configured to isocratic mode. The column used was a hydrophobic Kinetex 2.6  $\mu\text{m}$ , C18, 100 Å, 4.6 mm (Phenomenex), and the mobile phase was 55:45 (% v/v) RP-

HPLC grade CH<sub>3</sub>CN/Milli-Q. An injection sample volume of 90  $\mu\text{L}$  at a flow rate of 1.5 mL  $\text{min}^{-1}$  was used; each sample had a runtime of approximately 5 min at room temperature. The integral of the TX HPLC trace was then converted to concentration in order to evaluate the loss of surfactant. For the chemical analysis of NaDOC, electrospray ionization mass spectrometry (ESI-MS) was conducted on a Thermo Scientific LTQ-Orbitrap Velos mass spectrometer with the highest resolution setting of 100,000 ( $m/z$  400), in the positive ion mode. A solution of 40:60:0.1 (% v/v) (sample:MS grade CH<sub>3</sub>CN:HCO<sub>2</sub>H) was prepared and injected at 0.5  $\mu\text{L}$   $\text{min}^{-1}$  using an electrospray voltage of 3.8 kV. The mass spectra were acquired for 3 min, and the mass spectrometer was programmed to collect up to a maximum Orbitrap injection time of 500 ms, using an automatic gain control (AGC) setting of  $5 \times 10^5$ . The AGC is designed to fill the trap with the optimal amount of ions to ensure that the signal intensities are high and that the spectra are not distorted by space-charging effects. Estimates of the molecular fragment structures were performed using XCalibur (Thermo Scientific) software set to a mass accuracy of 5 ppm.

**Rheology Measurements.** Measurements were taken using a (AR-G2, TA Instruments) rheometer at 23 °C, with a rotational plate applying a cyclic shear rate of 50  $\text{s}^{-1}$  to 200  $\text{s}^{-1}$ .

## C. RESULTS AND DISCUSSION

**Cavitation Measurements.** In this work a unique acoustic measurement facility was established to achieve controlled ultrasonic conditions within the experimental solution volume. The ultrasonic source used was a 25 kHz-driven reference vessel<sup>16</sup> (Figure 1a), which was designed to produce repeatable acoustic cavitation of a known spatial distribution. The experimental solution was placed within the custom-built reactor (Figure 1b) located on the cylindrical vessel's central

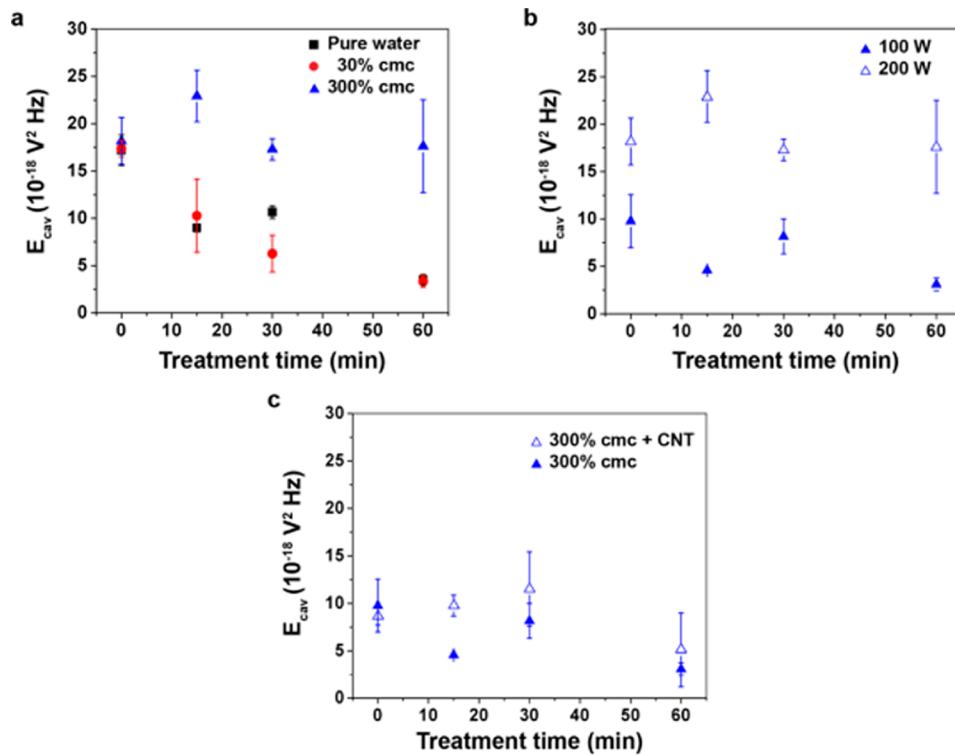


**Figure 2.** *In situ* cavitation measurements. **a**, Cavitation activity as a function of time for different surfactant (NaDOC) concentrations in the absence of CNTs during 60 min tests at 200 W. **b**, Cavitation activity as a function of time for different input powers for the 300% cmc solutions in the absence of CNTs. **c**, Cavitation activity as a function of time at 100 W for a 300% cmc solution in the absence and presence of 0.02 mg mL<sup>-1</sup> CNTs.

axis. The NPL cavitation sensor (Figure 1c) was housed in the reactor to measure the acoustic emissions from bubbles generated within the experimental volume. Key features of the frequency spectra, measured as a function of nominal electrical input power, are depicted in Figures 1d and 1e. At low input power a low driving acoustic pressure amplitude causes the bubble wall to oscillate linearly and only the fundamental driving frequency ( $f_0 = 25$  kHz) is observed. The degree of nonlinear oscillation increases as a function of driving pressure (typically via the increase of input electrical power), leading to the generation of various additional peaks,<sup>10,17</sup> among which is the first subharmonic, observed here at  $f_0/2 = 12.5$  kHz (Figure 1d). Further increases to the driving pressure lead to chaotic bubble oscillation and ultimately bubble collapse, which is demonstrated by the rising broadband noise level well into the MHz region (Figure 1e). It is generally accepted<sup>10</sup> that this broadband noise is associated with inertial (also known as transient) cavitation (Figure 1f), whereby bubbles collapse chaotically within a few pressure wave cycles. This is in contrast to stable cavitation (Figure 1f), whereby bubbles undergo multiple oscillations and do not necessarily collapse but can grow and be forced out of the liquid volume due to buoyancy.<sup>18</sup> The presence of the subharmonic peak, even at the lowest input power used in this work, indicates that the acoustic pressure amplitude in the selected measurement region is close to the inertial cavitation threshold. However there remains some debate over whether the amplitude of the subharmonic peak can be used as a measure of inertial cavitation,<sup>10</sup> and therefore a more definitive metric is required.

Studies of the high frequency (MHz) region have shown that the energy associated with the broadband acoustic emission spectrum is a practical metric for inertial cavitation activity.<sup>17</sup> This is parametrized by the term  $E_{\text{cav}}$ , which is evaluated by

integrating the square of the magnitude of the sensor response,  $V_c(f)^2$ , between two frequencies  $f_1$  and  $f_2$ , chosen to ensure that a significant fraction of the acoustic energy residing in the MHz region is acquired.

$$E_{\text{cav}} = \int_{f_1}^{f_2} V_c(f)^2 df \quad (1)$$

Measurements of  $E_{\text{cav}}$  in the frequency range of 2 to 4 MHz are shown in Figure 2 with additional data shown in Figure S2. The reactor experiments were performed using aqueous anionic surfactant sodium deoxycholate (NaDOC) solution, which is known to facilitate improved dispersion of SW-CNTs.<sup>7,19</sup> Tests were conducted with and without CNTs.<sup>20</sup> The effect of surfactant concentration on the acoustic field above (300%) and below (30%) the critical micelle concentration (cmc) of NaDOC was investigated by measurement of the cavitation activity.

No significant difference is observed between  $E_{\text{cav}}$  measurements in pure water and those in 30% cmc surfactant (Figure 2a), which suggests that the population of inertial cavitation bubbles at 30% cmc is similar to that found in pure water and that any excess bubbles are experiencing stable cavitation. The error bars indicate the short-time measurement variability associated with the stochastic nature of inertial cavitation. By contrast, after 60 min of ultrasonication the level of inertial cavitation at 300% cmc is significantly higher than that at 30% cmc, for example by approximately a factor of 4 at 200 W. This observation highlights the remarkable sensitivity of cavitation activity to solution composition. Since a negligible background activity was observed at 0 W, a nonlinear relationship exists between inertial cavitation activity and nominal input power (Figure 2b), highlighting an intrinsic limitation in the

widespread use of input power as a primary experimental parameter. A similar nonlinear behavior is evident in the broadband response shown in Figure 1d. No significant effect of the presence of CNTs was observed in the cavitation measurements (Figure 2c) under these conditions, which implies that the CNT concentration used in this study was sufficiently low that the measured acoustic field was relatively unperturbed.

A notable feature of the data in Figure 2a is that the magnitude of  $E_{\text{cav}}$  remains relatively constant for the 300% cmc solution but decreases with exposure time in both pure water and in 30% cmc solution. Inertial cavitation is clearly favored at the higher surfactant concentration, which may be ascribed to more facile formation of bubbles due to the reduced surface tension. Furthermore it is believed that at 30% cmc the distance between bubbles is relatively large due to electrostatic repulsion.<sup>21</sup> When the ionic surfactant concentration is increased to 300% cmc, the concomitant increase in solution ionic strength leads to charge shielding effects, reducing the repulsion between surfactant molecules and resulting in the formation of denser bubble clouds. A similar hypothesis was previously proposed to rationalize acoustic measurements in an anionic surfactant.<sup>21</sup> A contributing factor to the decrease in inertial cavitation with time in pure water and at 30% cmc may be a preference for stable cavitation as the bulk solution temperature increases during ultrasonication.<sup>9,11</sup>

The average variation of solution temperature during ultrasonication at 200 W is shown in Figure 3. The temperature

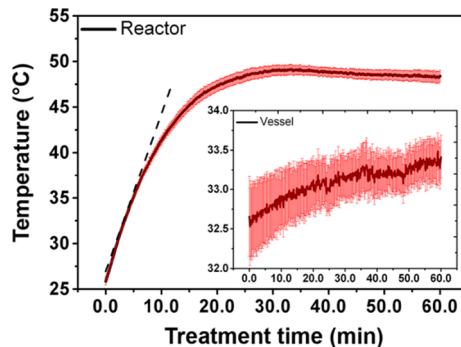


**Figure 3.** Average thermographs of the temperature within the reactor during the 200 W tests. Inset illustrates the vessel temperature profile. Error bars represent standard error between six independent measurements.

increases from its initial value of  $\sim 25$  °C and reaches a steady state value of  $\sim 48$  °C after approximately 30 min; a similar trend is observed at 100 W (see Figure S3) with a lower steady state temperature of  $\sim 41$  °C. This temperature increase will enhance bubble formation due to the increase of vapor pressure. However at 30% cmc the more widely spaced bubbles will grow via the mechanism of rectified diffusion,<sup>9</sup> whereby growth is achieved as a result of uneven mass transfer across the bubble/solution interface. Degassing can then occur via bubble coalescence and removal from the liquid due to buoyancy, hence reducing the number of bubble nucleation sites. By contrast, the 300% cmc solution could enhance the number of cavitation nucleation sites due to the high concentration of micelles. In addition, the use of a low frequency device (25 kHz) will favor a more significant increase in the population of bubbles undergoing inertial cavitation at the higher surfactant

concentration.<sup>22</sup> This effect is enhanced by the denser bubble population at 300% cmc.

The fraction of the nominal input power that is converted to thermal energy may be determined by calorimetric analysis of the thermographs (see the Supporting Information). At 100 W, 35% of the input power is converted to heat; this falls to 25% at 200 W. No linear dependence of amount of cavitation on the input thermal energy was observed, implying that input thermal power is an equally unsatisfactory indicator of the amount of cavitation in solution. This nonlinearity is due to nonuniformities in the acoustic field partially arising from system geometry and the acoustic properties of the container material. Other indirect metrics for cavitation level such as energy density have been proposed in the literature,<sup>23</sup> but this study demonstrates that caution should be applied to the use of any metric that is based on calorimetric determination of the acoustic energy. For example, if the cavitation distribution is nonuniform in the treated volume, a comparison of two systems based on calorimetric measurement may be misleading.

**Comparison with Tip Ultrasonication.** Routine approaches to CNT dispersion often utilize an ultrasonic tip, as opposed to a bath, so it is pertinent to compare the  $E_{\text{cav}}$  values from the reference vessel with those obtained from a commonly used benchtop sonotrode. As shown in Figure 4, a maximum in

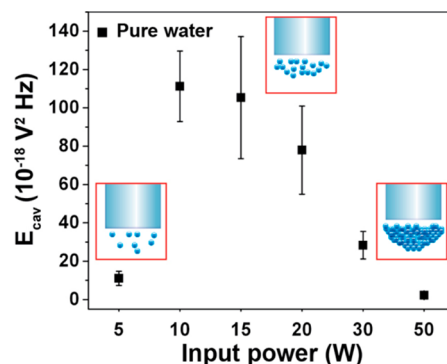


**Figure 4.** Cavitation activity measured for a tip ultrasonic device as a function of input power. Insets illustrate the variation of bubble population in the vicinity of the tip in three distinct regions of the graph. Error bars represent standard error between four to eight independent measurements.

$E_{\text{cav}}$  is reached between 10 and 15 W before a steady decline of cavitation activity is observed, approaching background levels at 50 W. The decrease in  $E_{\text{cav}}$  with increasing input power is due to cavitation shielding,<sup>11</sup> where the increasing population of coalescing bubbles immediately beneath the tip leads to formation of air pockets surrounded by a stagnant region.

This hinders the transmission of acoustic waves and the generation of inertial cavitation. The nonlinear response with input power and its potential variation across ultrasonication devices present a barrier to the intelligent selection of treatment parameters. The  $E_{\text{cav}}$  levels determined in the sonotrode and reactor measurements may be compared directly, as they are made with the same sensor, in the same container, and with a similar medium. The peak  $E_{\text{cav}}$  levels observed with the sonotrode are approximately an order of magnitude higher than in the reactor, which shows that even at modest input powers tip sonication is significantly disruptive. The sonotrode output is applied directly to the fluid through a 15 mm diameter tip, which vibrates with a displacement of up to 15  $\mu\text{m}$ . This

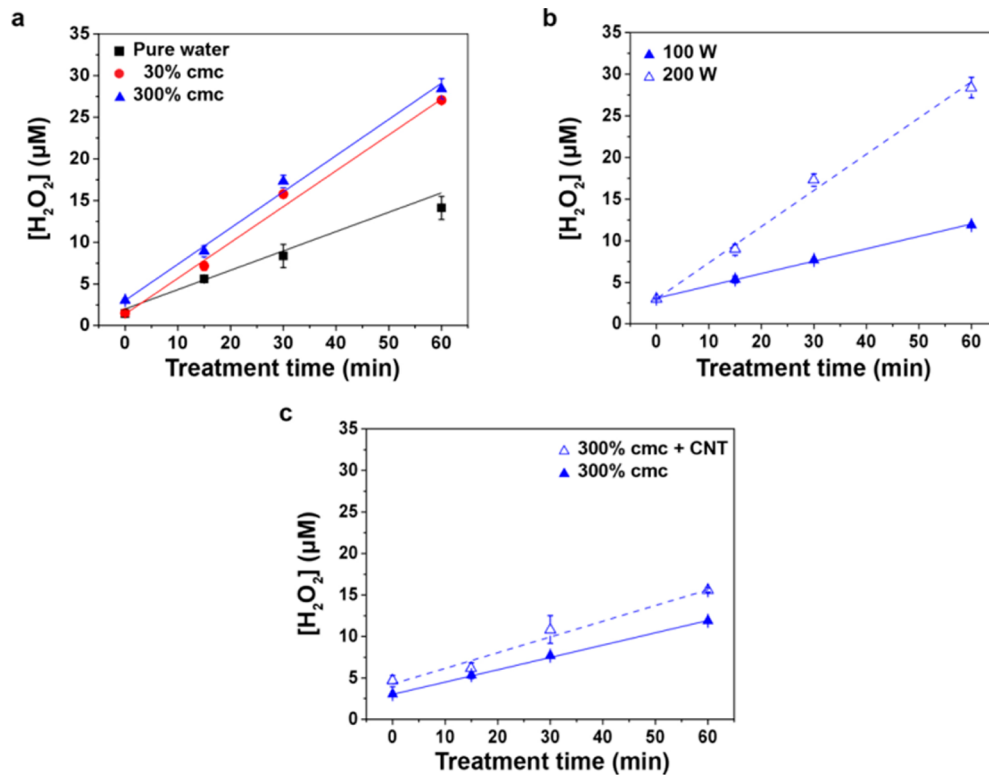


**Figure 5.** Sonochemical generation of hydrogen peroxide. **a**,  $\text{H}_2\text{O}_2$  concentration as a function of time for different surfactant concentrations in the absence of CNTs during 60 min tests at 200 W. **b**,  $\text{H}_2\text{O}_2$  concentration as a function of time for different input powers for the 300% cmc solutions in the absence of CNTs. **c**,  $\text{H}_2\text{O}_2$  concentration as a function of time at 100 W for a 300% cmc solution in the absence and presence of 0.02 mg mL<sup>-1</sup> CNTs. Error bars represent standard error between four independent measurements.

generates locally high acoustic pressures, which in turn cause intense inertial cavitation, but over a very small region, i.e. a few millimeters below the tip. For equivalent powers, the reactor wall displaces less than 1  $\mu\text{m}$  but still generates acoustic pressures sufficient to cause inertial cavitation over a much larger fluid volume. With the acoustic field and the consequent cavitation activity generated by a larger number of acoustic sources, i.e. the vessel's ten equidistantly spaced transducers, a more even cavitation field is generated and the likelihood of cavitation shielding is reduced. Thus, the reactor generates a far more uniform cavitation distribution than the sonotrode and potentially a better 'nanoparticle dispersion stimulus' within a larger solution volume. The sonotrode has the additional disadvantage of contamination of the solution with metal fragments eroded from the tip.<sup>11</sup> These considerations point to significant advantages for industrial scale-up of such batch processing.

**Hydrogen Peroxide Measurements.** Measurement of reactive oxygen species (ROS) such as hydrogen peroxide ( $\text{H}_2\text{O}_2$ ) generated by ultrasonication can be used as a quantitative indicator of cavitation activity.<sup>9,11</sup> The cumulative concentration of  $\text{H}_2\text{O}_2$  measured under the same conditions as the *in situ* acoustic measurements is presented in Figure 5 with additional data shown in the Supporting Information (Figure S4). In all cases a linear trend of  $\text{H}_2\text{O}_2$  concentration with time is observed. The results are in marked contrast to the acoustic data in Figure 2. First, the most significant change in the rate of production of  $\text{H}_2\text{O}_2$  is observed between pure water and the 30% cmc solution, rather than between the two surfactant concentrations (Figure 5a). Second, the rate of generation of  $\text{H}_2\text{O}_2$  varies approximately linearly with input power (Figure

Sb). Third, an effect (albeit modest) of CNT presence is observed (Figure 5c).

The apparent discrepancy between the acoustic data and the  $\text{H}_2\text{O}_2$  concentration measurements may be explained on the basis of inertial vs stable cavitation. The highly spaced bubbles in the 30% cmc solution will undergo stable cavitation activity assisted by the thermal effects discussed above and act as microreactors for  $\text{H}_2\text{O}_2$  formation,<sup>24</sup> which explains the marked increase of  $\text{H}_2\text{O}_2$  generation compared to pure water. Importantly this does not exclude the formation of inertial bubbles, since higher than background activities were recorded (Figure 2a).

These observations suggest that the predominant route to  $\text{H}_2\text{O}_2$  formation is in fact stable cavitation, as opposed to inertial cavitation, and that the excess surfactant might behave as a primary micelle radical trap<sup>21</sup> or radical scavenger,<sup>25</sup> as evidenced by the comparably small apparent increase in  $\text{H}_2\text{O}_2$  formation between 30% and 300% cmc surfactant. The relatively small systematic increase in  $\text{H}_2\text{O}_2$  concentration due to the presence of CNTs (Figure 5c) suggests that the CNTs (at the low concentration used in this work) have only a minor role in the formation of bubbles undergoing stable cavitation. Trapped air within the CNT agglomerates released during debundling, coupled with the increased number of nucleation sites due to the additional surface area, may in fact provide additional sources of stable cavitation.

**Surfactant Degradation.** Another key finding of our study is the degradation of surfactant as a result of ultrasonication. Chemical characterization of 2% cmc NaDOC solution using mass spectroscopy (MS) demonstrates the growth of new molecular fragments and their increase in concentration with

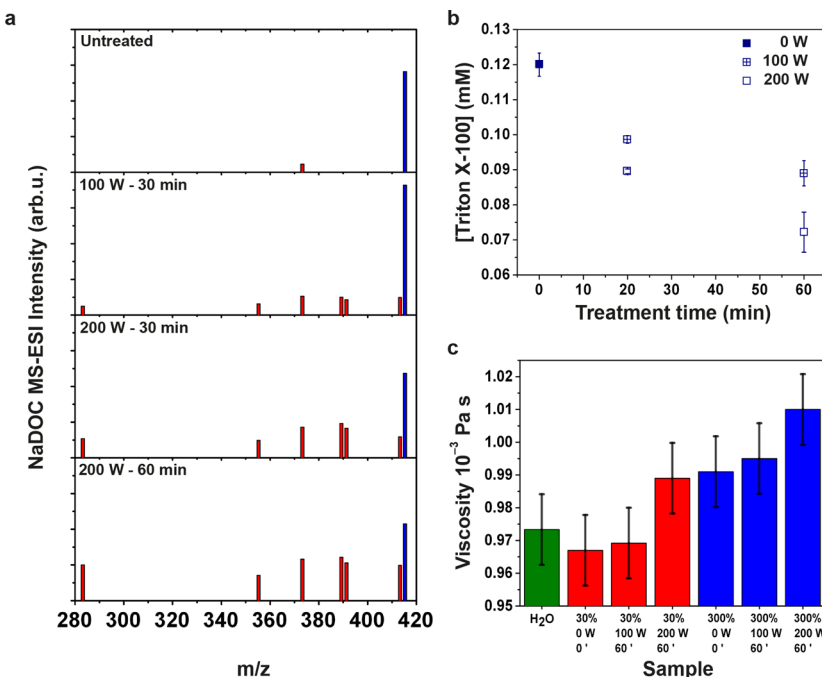


**Figure 6.** Sonochemical effects on two common CNT-dispersing surfactants. **a**, ESI-MS analysis of aqueous solutions of NaDOC (blue), showing the generation of smaller molecular fragments (red) over time as a result of ultrasonication. Top inset illustrates the molecular structure of the pristine NaDOC molecule; bottom inset illustrates the proposed degradation reaction scheme for the oxidative dehydrogenation and dehydration of NaDOC. **b**, HPLC analysis of aqueous solutions of TX as a function of ultrasonication time for different applied powers. Inset illustrates the molecular structure of the pristine TX molecule. **c**, Dynamic viscosity measurements of NaDOC solutions compared to that of pure water. Error bars represent standard error between four independent measurements.

ultrasonication time and input power (Figure 6a). These fragments can be assigned to specific products (see Table S1) resulting from the oxidative dehydrogenation and dehydration of the parent NaDOC molecule, initiated by ROS. Similar damage is observed to a nonionic surfactant, TX, which is also commonly used in the literature as a CNT dispersant. In this case the HPLC analysis indicated a gradual decrease in TX concentration when subjected to ultrasonication (Figure 6b). The reduction in spectral intensity with increasing exposure time and input power can be attributed to the degradation of the chromophore-bearing hydrophobic segment (Figure S5). A similar process is used in water treatment to destroy undesirable surfactants via pyrolytic bond cleavage and ROS chemical attack,<sup>26</sup> although this typically employs much higher frequencies (hundreds of kHz). Our results show that ultrasonic degradation of surfactants is clearly also an issue of concern at lower frequencies and its exact impact on dispersion efficiency will require more detailed studies of surfactant-CNT surface interactions as demonstrated elsewhere.<sup>27</sup> However, at 30% cmc and 300% cmc of NaDOC no distinctive fragments were observed in the MS analysis, which may be a result of the increased turbidity of these solutions as discussed below.

Visual observation of the surfactant–water solutions (i.e., in the absence of CNTs) revealed a steadily increasing turbidity with ultrasonication time. To our knowledge this effect has not been previously reported in the literature on CNT dispersion, most likely because CNTs are always present in such studies, typically at relatively high concentrations. Turbidity of a surfactant solution may occur as a result of the dehydration of the hydrophilic segment of the surfactant as the bulk solution temperature increases, leading to the formation of close packed structures and phase separation within the liquid.<sup>28</sup> This behavior raises a number of questions regarding the

effectiveness of NaDOC as a CNT dispersant as well as its effect on bubble dynamics. Rheology measurements showed a correlation between the extent of ultrasonic treatment and viscosity (Figure 6c). The magnitude of the increase in viscosity was modest in absolute terms, with a maximum of ~4% for the higher surfactant concentration after 60 min at 200 W. Nevertheless, a trend with increasing exposure conditions can be discerned.

**Carbon Nanotube Dispersion.** The phase behavior of CNT dispersion is complex in nature.<sup>27</sup> In particular, aqueous based dispersions which use surfactant as a stabilizer require a subtle balance between surfactant and CNT concentrations. Often, dispersions that have been subjected to extended ultrasonication are unstable over time with the result that the CNTs eventually sediment out of solution. This is illustrated in Figure 7a, which depicts 30% cmc (right vial) and 300% cmc (left vial) solution left standing for 14 days after ultrasonication for 60 min at 200 W. Whereas a uniform dispersion was maintained in the 300% cmc surfactant solution, significant sedimentation was observed at 30% cmc, indicating the critical role of the surfactant concentration. UV-vis absorption spectroscopy may be used to characterize the quality of the CNT dispersion,<sup>29</sup> typically via the analysis of the resonance peak ratio.<sup>30</sup> This is depicted in Figure 7b for the two different surfactant concentrations treated at 200 W.

The drop observed from 0 to 15 min illustrates the reagglomeration and sedimentation of the CNTs, which failed to disperse when the pretreated solution was stirred into the remaining reactor volume (see the Experimental Section). Therefore, the dispersion is not at equilibrium and is dynamically changing; the resulting flocculation can occur via depletion driven aggregation,<sup>27</sup> which depends on surfactant concentration as well as the interaction of the surfactant with

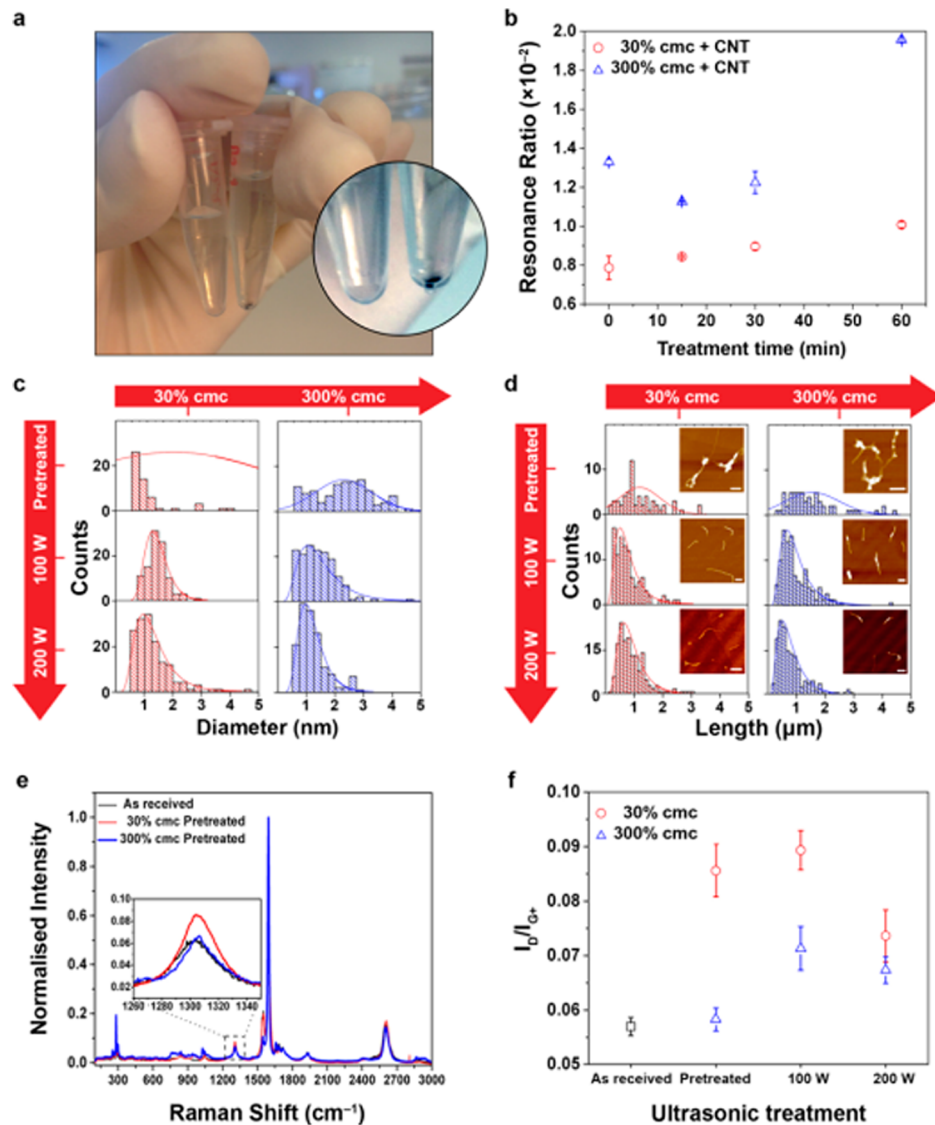


**Figure 7.** Characterization of CNT quality and dispersion. **a**, Photograph illustrating effect of surfactant concentration on CNT dispersion stability (left vial: 300% cmc, right vial: 30% cmc NaDOC). **b**, Optical absorption resonance ratio of the  $E_{22}$  resonance band for ultrasonically treated CNTs, indicating an increase in the concentration of singly dispersed CNTs as a function of applied power and exposure time. **c**, CNT diameter measurements from AFM images of mica substrates spin-coated with solutions ultrasonically treated for 60 min as a function of surfactant concentration and input power. **d**, CNT length measurements from AFM images of mica substrates spin-coated with solutions ultrasonically treated for 60 min as a function of surfactant concentration and input power. Scale bars: 400 nm. **e**, Representative Raman spectra of dried CNTs before and after pretreatment. **f**, Raman spectroscopy quality ratios ( $I_D/I_{G^+}$ ) for as-received and ultrasonically treated CNTs. Error bars represent standard error between four independent measurements.

the CNT lattice. Readings taken from 15 min onward clearly show a gradual increase in the population of dispersed CNTs. A similar trend is observed at 100 W (Figure S6a). The 10-fold increase of surfactant concentration leads to the exfoliation of more CNTs, with an average increase in dispersion efficiency of ~25% at 100 W and ~80% at 200 W (Figure S6b and S6c respectively). CNT diameter and length histograms were determined from detailed analysis of representative AFM images after 60 min of exposure. Both exfoliation (Figure 7c) and length reduction (Figure 7d) are evident, with the reduction in CNT diameter and length more pronounced at 300% cmc and 200 W. The pretreated solutions are populated by a range of bundle sizes, up to 30 nm at 30% cmc and <10 nm at 300% cmc. The effect of ultrasonication is to reduce the average bundle diameter significantly, to below 5 nm at 30% cmc and to below 3 nm at 300% cmc. Similar effects are

observed on CNT length, for which the largest effect is observed at 300% cmc, with a ~36% average reduction in CNT length at 200 W within 60 min, compared to ~27% for all other exposures. The AFM data are summarized in an alternative format in Figure S7.

Raman spectroscopy is used to determine the increase in defects<sup>31</sup> created by ultrasonication, indicated by the intensity ratio of the D-band to the G<sup>+</sup>-band ( $I_D/I_{G^+}$ ) as shown in the representative spectra in Figure 7e. Significant damage to the CNTs is observed during pretreatment at 30% cmc but not at 300% cmc (Figure 7f). The general observation that the  $I_D/I_{G^+}$  ratio is affected by ultrasonication may be related to CNT damage via ROS attack.<sup>32</sup> The lower level of damage at 300% cmc is rationalized by the protective coating of the excess surfactant on the CNT surface, which will naturally form as the cmc point is surpassed. Interestingly, the  $I_D/I_{G^+}$  ratio is lower at

200 W than at 100 W for both surfactant concentrations, which is more marked for the 30% cmc sample. The AFM analysis indicates that the change in average length distribution between the two powers is not sufficient to explain the reduction in this ratio. It may however be a result of disruption of the long-range order of the  $sp^2$  carbon hexagonal as the number of point-like defect sites increases.<sup>33</sup>

**Implications.** The acoustic and sonochemical measurements discussed above have significant implications for researchers wishing to control dispersion of nanomaterials for a wide range of applications. Ultrasonic processing remains the primary dispersion technique for CNTs and other nanoparticles but the rather ad hoc approach to most processes in the literature has major ramifications for reproducibility and dispersion quality. Measurement and control of acoustic cavitation, rather than application of an arbitrary input power, are required to achieve control of nanomaterial dispersion. In the case of CNTs, we conclude that the enhanced exfoliation and length reduction is a result of inertial cavitation, whereas sonochemically induced surface damage is associated with stable cavitation. Dispersion of CNTs in aqueous solution is dominated by mechanical forces generated via inertial cavitation, which depends critically on surfactant concentration. Our approach can be readily generalized to other nanomaterials, for instance 2D layered materials such as graphene and MoS<sub>2</sub>, whose physical and chemical properties are particularly sensitive to number of layers and flake size.<sup>1</sup>

From a practical standpoint, careful consideration should be given to container material and vessel geometry when using bath sonication. The use of tip sonication is more challenging due to its intrinsic nonlinearity, cavitation shielding effects, and volume limitations. For large scale processing, use of a bath vessel with well-controlled and uniform cavitation such as that used in this work is required.

## D. CONCLUSIONS

We have developed a new approach for producing a well-characterized acoustic cavitation field during ultrasonication of CNTs, to improve control of dispersion. Through a unique measurement technique, based on *in situ* broadband acoustic emission monitoring and H<sub>2</sub>O<sub>2</sub> production, we distinguish between two different cavitation types: (i) stable cavitation, which leads to chemical attack on the CNTs, and (ii) inertial cavitation, which favors CNT exfoliation and length reduction. The control of CNT dispersion is more challenging with a tip ultrasonicator due to its intrinsic nonlinearity and the presence of cavitation shielding effects. Care must be exercised when using tip-based ultrasonication as the local fields are much higher. We have also highlighted surfactant degradation in the water–surfactant control system in the tens of kHz frequency range used for routine ultrasonication of CNTs. Furthermore, the surfactant concentration has a profound effect on cavitation activity and resulting dispersion quality via modification of bubble surface tension, radical scavenging, and protective coating of CNTs. The bulk solution temperature increases with time during ultrasonication and has a major influence on the dispersion efficiency through increased vapor pressure and changes in surfactant and bubble dynamics. This study demonstrates that measurement and control of acoustic cavitation rather than blind application of input power is critical in the ultrasonic dispersion of nanomaterials with tailored properties. The results have major implications for

enhanced control and scale-up of nanoparticle dispersion using ultrasonic processing.

## ■ ASSOCIATED CONTENT

### § Supporting Information

Schematic of experimental set up; additional cavitation measurements; estimation of effective power; additional H<sub>2</sub>O<sub>2</sub> measurements; sonochemical degradation of surfactants; additional UV–vis absorption spectroscopy measurements; AFM data analysis. This material is available free of charge via the Internet at <http://pubs.acs.org>.

## ■ AUTHOR INFORMATION

### Corresponding Author

\*Phone: + 44 20 8943 7147. E-mail: gareth.hinds@npl.co.uk.

### Notes

The authors declare no competing financial interest.

## ■ ACKNOWLEDGMENTS

This work was supported by the U.K. National Measurement System (NMS) under the Innovation R&D Programme and by the U.K. Engineering and Physical Sciences Research Council (EPSRC) under the Industrial Doctorate Engineering Programme in Micro- and NanoMaterials and Technologies at the University of Surrey. The authors thank NPL scientific staff members Dr. B. Zeqiri, Dr. J. Nunn, Mr. C. Allen, Ms. T. L. Salter, Dr. E. Cerasoli, Dr. T. Sainsbury, and Dr. M. O'Connell for useful discussions and technical assistance in sample preparation and data analysis; Dr. J. A. Fagan from the US National Institute of Standards and Technology for contributing the CNTs; Mr. D. Lamprou from the University of Surrey for his C.A.D. technical drawing assistance; and the NPL Reprographics team for their assistance with the figures.

## ■ REFERENCES

- (1) Coleman, J. N.; et al. Two-Dimensional Nanosheets Produced by Liquid Exfoliation of Layered Materials. *Science* **2011**, *331*, 568–571.
- (2) Nie, Z.; Petukhova, A.; Kumacheva, E. Properties and Emerging Applications of Self-Assembled Structures Made From Inorganic Nanoparticles. *Nature Nanotechnol.* **2010**, *5*, 15–25.
- (3) Tománek, D.; Jorio, A.; Dresselhaus, M. S.; Dresselhaus, G. Introduction to Important and Exciting Aspects of Carbon-Nanotube Science and Technology. In *Carbon nanotubes: Advanced Topics In The Synthesis, Structure, Properties And Applications*; Jorio, A., Dresselhaus, M. S., Dresselhaus, G., Eds.; Topics in Applied Physics 111; Springer-Verlag: Berlin, 2008; pp 1–12.
- (4) De Volder, M. F. L.; Tawfick, S. H.; Baughman, R. H.; Hart, A. J. Carbon Nanotubes: Present and Future Commercial Applications. *Science* **2013**, *339*, 535–539.
- (5) Schneeweiss, P.; Gierling, M.; Visanescu, G.; Kern, D. P.; Judd, T. E.; Günther, A.; Fortágh, J. Dispersion Forces Between Ultracold Atoms and A Carbon Nanotube. *Nat. Nanotechnol.* **2012**, *7*, 515–519.
- (6) Coleman, J. N. Liquid-Phase Exfoliation of Nanotubes and Graphene. *Adv. Funct. Mater.* **2009**, *19*, 3680–3695.
- (7) Blanch, A. J.; Lenehan, C. E.; Quinton, J. S. Optimizing Surfactant Concentrations for Dispersion of Single-Walled Carbon Nanotubes in Aqueous Solution. *J. Phys. Chem. B* **2010**, *114*, 9805–9811.
- (8) Leighton, T. G. What is Ultrasound? *Prog. Biophys. Mol. Biol.* **2007**, *93*, 3–83.
- (9) Roy, R. A. Cavitation Sonophysics. In *Sonochemistry and Sonoluminescence*; Crum, L. A., Mason, T. J., Reisse, J. L., Suslick, K. S., Eds.; Series C: Mathematical and Physical Sciences – Vol. 524; Kluwer Academic Publishers: Dordrecht, 1999; pp 25–38.

- (10) Lauterborn, W.; Kurz, T. Physics of Bubble Oscillation. *Rep. Prog. Phys.* **2010**, *73*, 106501–106589.
- (11) Sutkar, V. S.; Gogate, P. R. Design Aspects of Sonochemical Reactors: Techniques for Understanding Cavitation Activity Distribution and Effect of Operating Parameters. *Chem. Eng.* **2009**, *155*, 26–36.
- (12) Paganin, G.; Green, M. J.; Poulin, P.; Pasquali, M. Competing Mechanisms and Scaling Laws for Carbon Nanotube Scission by Ultrasonication. *Proc. Natl. Acad. Sci. U. S. A.* **2012**, *109*, 11591–11604.
- (13) Green, M. J. Analysis and Measurement of Carbon Nanotube Dispersions: Nanodispersion vs. Macrodispersion. *Polym. Int.* **2010**, *5*, 1319–1322.
- (14) Xu, H.; Zeiger, B. W.; Suslick, K. S. Sonochemical Synthesis of Nanomaterials. *Chem. Soc. Rev.* **2013**, *42*, 2555–2567.
- (15) Taurozzi, J. S.; Hackley, V. A.; Wiesner, M. R. Ultrasonic Dispersion of Nanoparticles for Environmental, Health and Safety Assessment-Issues and Recommendations. *Nanotoxicology* **2010**, *5*, 711–729.
- (16) Memoli, G.; Gélat, P. N.; Hodnett, M.; Zeqiri, B. Characterisation and Improvement of A Reference Cylindrical Sonoreactor. *Ultrason. Sonochem.* **2012**, *19*, 939–952.
- (17) Hodnett, M.; Chow, R.; Zeqiri, B. High-Frequency Acoustic Emissions Generated by A 20 kHz Sonochemical Horn Processor Detected Using A Novel Broadband Acoustic Sensor: A Preliminary Study. *Ultrason. Sonochem.* **2004**, *11*, 441–454.
- (18) Ashokkumar, M.; Lee, J.; Kentish, S.; Grieser, F. Bubbles In an Acoustic Field: An Overview. *Ultrason. Sonochem.* **2007**, *14*, 470–475.
- (19) Wenseleers, W.; Vlasov, I. I.; Goovaerts, E.; Obraztsova, E. D.; Lobach, A. S.; Bouwen, A. Efficient Isolation and Solubilisation of Pristine Single-Walled Nanotubes in Bile Salt Micelles. *Adv. Funct. Mater.* **2004**, *14*, 1105–1112.
- (20) SRM®2483 Single-Wall Carbon Nanotubes (Raw soot) Certificate of analysis. Available at [http://www.nist.gov/mml/msed/complex\\_fluids/nanotube-reference-materials.cfm](http://www.nist.gov/mml/msed/complex_fluids/nanotube-reference-materials.cfm) (accessed August 2013).
- (21) Ashokkumar, M.; Hodnett, M.; Zeqiri, B.; Grieser, F.; Price, G. J. Acoustic Emission Spectra From 515 kHz Cavitation in Aqueous Solutions Containing Surface-Active Solutes. *J. Am. Chem. Soc.* **2007**, *129*, 2250–2258.
- (22) Ashokkumar, M.; Lee, J.; Iida, Y.; Yasui, K.; Kozuka, T.; Tuziuti, T.; Towata, A. The Detection and Control of Stable and Transient Acoustic Cavitation Bubbles. *Phys. Chem. Chem. Phys.* **2009**, *11*, 10118–10121.
- (23) Blanch, A. J.; Lenehan, C. E.; Quinton, J. S. Parametric Analysis of Sonication and Centrifugation Variables for Dispersion of Single Walled Carbon Nanotubes in Aqueous Solutions of Sodium Dodecylbenzene Sulfonate. *Carbon* **2011**, *49*, 5213–5228.
- (24) Tronson, R.; Ashokkumar, M.; Grieser, F. Comparison of the Effects of Water-Soluble Solutes on Multibubble Sonoluminescence Generated In Aqueous Solutions by 20- and 515-kHz Pulsed Ultrasound. *J. Phys. Chem. B* **2002**, *106*, 11064–11068.
- (25) Sostaric, J. Z.; Riesz, P. Adsorption of Surfactants at the Gas-Solution Interface of Cavitation Bubbles: An Ultrasound Intensity-Independent Frequency Effect in Sonochemistry. *J. Phys. Chem. B* **2002**, *106*, 12537–12548.
- (26) Destaillats, H.; Hung, H. M.; Hoffmann, M. R. Degradation of Alkyphenol Ethoxylate Surfactants in Water with Ultrasonic Irradiation. *Environ. Sci. Technol.* **2000**, *34*, 311–317.
- (27) Angelikopoulos, P.; Bock, H. The Science of Dispersing Carbon Nanotubes with Surfactants. *Phys. Chem. Chem. Phys.* **2012**, *14*, 9546–9557.
- (28) Mukherjee, P.; Padhan, S. K.; Dash, S.; Patel, S.; Mishra, B. K. Clouding Behaviour in Surfactant Systems. *Adv. Colloid Interface Sci.* **2011**, *162*, 59–79.
- (29) Naumov, A.; Ghosh, V. S.; Tsyboulski, D. A.; Bachilo, S. M.; Weisman, R. B. Analyzing Absorption Backgrounds in Single-Walled Carbon Nanotube Spectra. *ACS Nano* **2011**, *5*, 1639–1648.
- (30) Tan, Y.; Resasco, D. E. Dispersion of Single-Walled Carbon Nanotubes of Narrow Diameter Distribution. *J. Phys. Chem. B* **2005**, *109*, 14451–14460.
- (31) Jorio, A.; Dresselhaus, M. S.; Saito, R.; Dresselhaus, G. *Raman Spectroscopy in Graphene Related Systems*; Wiley-VCH: Weinheim, Germany, 2011.
- (32) Fenoglio, I.; Tomatis, M.; Lison, D.; Muller, J.; Fonseca, A.; Nagy, J. B.; Fubini, B. Reactivity of Carbon Nanotubes: Free Radical Generation or Scavenging Activity? *Free Radical Biol. Med.* **2006**, *40*, 1227–1233.
- (33) Cançado, L. G.; et al. Quantifying Defects in Graphene via Raman Spectroscopy at Different Excitation Energies. *Nano Lett.* **2011**, *11*, 3190–3196.